Ore Geology Reviews 159 (2023) 105560

Contents lists available at ScienceDirect

Ore Geology Reviews

journal homepage: www.elsevier.com/locate/oregeorev

A metasedimentary origin for gold deposits in the Dian-Qian-Gui "Golden Triangle" of Southwest China

Rucao Li [a,b], Qinping Tan [c], Xiao-Lei Wang [b,*], Xiaoming Sun [d], Tao Yang [b], Yong Xia [c], Yue Guan [b], Yuzhou Feng [e]

[a] College of Earth Science and Engineering, Shandong University of Science and Technology, Qingdao 266590, China
[b] State Key Laboratory for Mineral Deposits Research, School of Earth Sciences and Engineering, Nanjing University, Nanjing 210023, China
[c] State Key Laboratory of Ore Deposit Geochemistry, Institute of Geochemistry, Chinese Academy of Sciences, Guiyang 550002, China
[d] School of Marine Sciences, Sun Yat-sen University, Guangzhou 510006, China
[e] Guangzhou Institute of Geochemistry, Chinese Academy of Science, Guangzhou 510640, China

ARTICLE INFO

Keywords:
Metasedimentary origin
Golden triangle
Sulfur isotope
Co/Ni ratio
Pyrite

ABSTRACT

The Dian-Qian-Gui "Golden Triangle" area of Southwest China hosts a large number of Au deposits. However, the sources of the ore-forming fluids are still controversial, hampering the formulation of a sound genetic model and effective ore prospecting. Here we investigate the sources of ore-forming fluids by an integrated study of in-situ sulfur isotope analyses and available trace element (e.g., Co and Ni) data for the pyrite in the "Golden Triangle" area. We find that the ore stage pyrites are featured by low Co/Ni ratios (mostly < 2), which is distinct from pyrite formed in magmatic-hydrothermal systems but resemble typical sedimentary pyrite. In addition, the significant variation (from −7.5 to +20.0‰) in sulfur isotopes ($\delta^{34}S$) of the ore stage pyrite in these deposits also support a sedimentary origin of the ore-forming fluids. Considering the difference in sulfur isotopic compositions of ore-stage pyrite and the sedimentary host rocks, we suggest the metasedimentary basement rocks (>500 Ma) in the area may have supplied most of the sulfur and gold for the ore-forming fluids during the Triassic orogenesis in the Dian-Qian-Gui "Golden Triangle" area of Southwest China.

1. Introduction

The Dian-Qian-Gui "Golden Triangle" area of southwest China hosts numerous gold deposits that shows similarity with Carlin-type deposits (Su et al., 2018; Xie et al., 2018a) and possibly formed at conditions somewhat intermediate to that for Carlin-type deposits and orogenic systems (Cline et al., 2013). Key characteristics of the deposits include: (1) In most cases, Au is present as invisible gold that is ionically bounded in trace element-rich arsenian pyrite (Su et al., 2018; Xie et al., 2018b); (2) Orebodies are mostly hosted by carbonate-bearing rocks and are controlled by faults and/or anticlines (Tan et al., 2015a; Xie et al., 2018b); (3) Ore elements generally include Au, As, Cu, Sb, Hg and Tl, with low to no Ag and base metals; (4) The alteration features associated with Au-bearing pyrite include dissolution of calcite and sulfidation of Fe in Fe dolomite to form Au-bearing pyrite and dolomite (Su et al., 2009); (5) Stibnite, realgar, calcite, quartz, orpiment and cinnabar precipitated within veins during late ore stage (Tan et al., 2015a; Xie et al., 2018a); and (6) The deposits generally formed at depths between 2 and 8 km and at temperatures of 190 to 300 °C, and the ore-forming fluids are low-salinity (<5 wt% NaCl equiv) and CO_2-rich (6 to 75 mol %) (Su et al., 2018; Su et al., 2009).

Even though with many previous studies, source(s) of the ore-forming fluids remains controversial. Two main sources have been proposed: (1) magmatic fluids (Xie et al., 2018b); and (2) metamorphic fluids (Hofstra et al., 2005; Su et al., 2018). Magmatic sulfur generally has $\delta^{34}S$ range of −5 to +5‰ (e.g., Seal, 2006), while metamorphic sulfur could be highly variable in its $\delta^{34}S$ values (Goldfarb and Groves, 2015), indicating that sulfur isotope could possibly distinguish these two sources. Besides, sulfur has been suggested to be the principal ligand responsible for Au transport in Carlin-type systems (e.g., $Au(HS)^0$ and/or $Au(HS)_2^-$) (Cline et al., 2005 and references therein), and sulfur isotopes of ore stage pyrite, the main host of Au in "Golden Triangle" (Xie et al., 2018a and references therein), can also put critical constraints on the potential source(s) for Au.

The gold in the deposits of the "Golden triangle" area mostly occur as invisible gold that is hosted in the arsenian pyrite (Xie et al., 2018b), and

* Corresponding author.
E-mail address: wxl@nju.edu.cn (X.-L. Wang).

https://doi.org/10.1016/j.oregeorev.2023.105560
Received 23 March 2023; Received in revised form 18 June 2023; Accepted 20 June 2023
Available online 23 June 2023

sulfur isotopic investigations have been made on these pyrites to trace potential fluid source(s). However, gold-bearing pyrites in this area generally have multiple generations in one grain (e.g., He et al., 2021; Xie et al., 2018a) and bulk analysis very likely represents a mixture of pyrites of different stages (e.g., Tan et al., 2015b), which makes previously published bulk sulfur isotope data fail to provide creditable information on the sources of Au-bearing fluids.

Indeed, the advantages of in-situ analyzing techniques (e.g., laser ablation-multicollector-inductively coupled plasma-mass spectrometry (LA-MC-ICP-MS) and secondary ion mass spectrometry (SIMS)) have enabled researchers to obtain high quality sulfur isotope results with high spatial resolution (e.g., with analysis spot of 10–50 μm). Based on an early compilation of in-situ sulfur isotopic results in the study area, Xie et al. (2018b) found a limited $\delta^{34}S$ range of −5 to +5‰ for the ore stage pyrites and suggested a magmatic origin for the ore-forming fluids. However, the subsequent in-situ sulfur isotope data suggest a more significant variation of $\delta^{34}S$ values for the ore stage pyrite in this area (e.g., Xie et al., 2018b; Yan et al., 2018), which challenges the previous magmatic model.

To re-assess the sources of Au deposits in the "Golden Triangle" area of SW China, this contribution obtained a new set of in-situ sulfur isotope data of pyrite from the two largest deposits in this area (i.e., Shuiyindong and Lannigou), and carried out an updated compilation of the published (in-situ) sulfur isotope together with trace element (i.e., Co and Ni) data of pyrite with clear texture information. With the results mentioned above, we discussed the potential source for the ore-forming fluids and materials.

2. Geology of sediment-hosted Au deposits in the "Golden Triangle" area

2.1. Regional geology

The Carlin-like gold deposits in the "Golden Triangle" area are restricted to the Youjiang Basin, which is bounded to the northwest by the Mile-Shizong fault, the northeast by the Ziyun-Du'an fault, and the southeast by the Pingxiang fault (Fig. 1) (Chen et al., 2011). Additionally, the basin is separated from the Simao Block by the Honghe Fault.

The ages of (meta)sedimentary rocks in the "Golden Triangle" area range from Neoproterozoic to Neogene (Chen, 2010; Cui et al., 2018; Shu et al., 2021), with a total thickness >13,500 m (Chen, 2010). The low greenschist facies-metamorphosed Banxi Group (~800 Ma) represents the observed oldest basement in the area (Chen, 2010), and it is mainly composed of shallow marine rocks and minor volcaniclastic rocks. It is overlain by the low- to non-metamorphosed Ediacaran to Middle Triassic marine face rocks and Late Triassic to Neogene terrestrial rocks (Chen, 2010; Jin, 2017). The unconformably overlaying Ediacaran to Silurian strata consist of carbonate rocks with minor sandstone and mudstone rocks (Chen, 2010; Jin, 2017), which is in turn overlain by Devonian-Triassic sandstone, siltstone and shale (Hou et al., 2016). The Middle Triassic strata is composed of shelf carbonates and abyssal siliciclastic turbidite. Gold deposits in this area generally occur

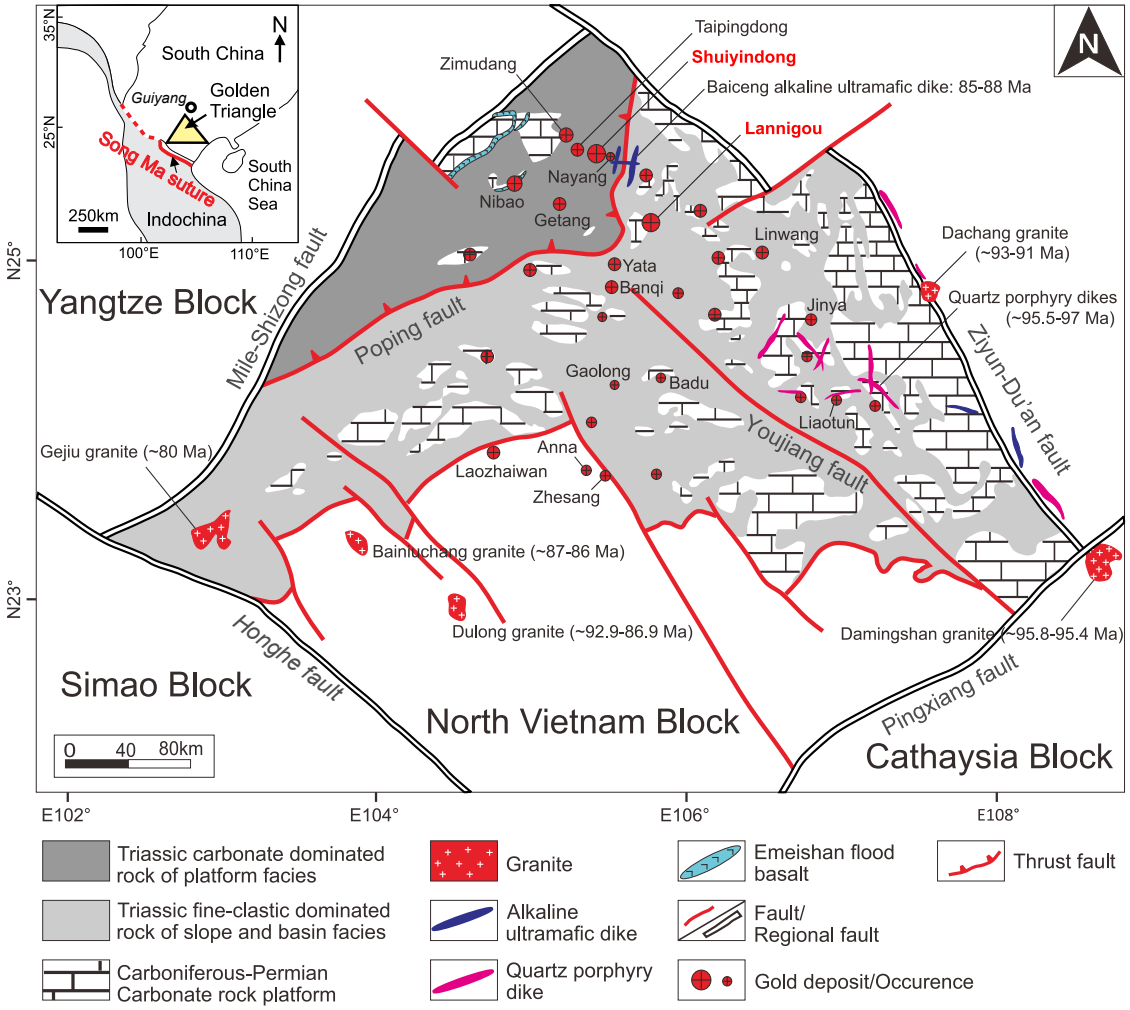

Fig. 1. Regional geologic map showing the distribution of sediment-hosted Au deposits in the "Golden Triangle" region. (Modified from Chen et al., 2011, Jin et al., 2021, Xie et al., 2018b).

in the Upper Permian-Middle Triassic strata that consist of bioclastic limestone and siltstone (Su et al., 2009; Wang et al., 1995), with a less number of them hosted by the Late-Permian diabase intrusions (e.g., Zhesang, Badu and Anna) (Dong et al., 2017; Pi et al., 2017; Su et al., 2018).

2.2. Deposit geology

Shuiyindong is the largest carbonate-hosted gold deposit in this area, with a gold reserve of 263 t (8.5 Moz) and an average gold grade of 5.0 g/t (0.2 oz/t) (Tan et al., 2015a). Lannigou is the second largest sediment-hosted gold deposit in this area, with a probable Au reserve of 110 t (3.6 Moz) and an average gold grade of 3.8 g/t (0.1 oz/t). Detailed deposit geology of the Shuiyindong and Lannigou has been described before (Su et al., 2018; Tan et al., 2015a; Xie et al., 2018b), and are summarized briefly as follows.

The Shuiyindong deposit is controlled by the ~5 km wide and ~20 km long Huijiabao anticline (Fig. 2). The strata presented at the Shuiyindong deposit includes bioclastic limestone of the Middle Permian Maokou Formation, interbedded sandstone, siltstone, limestone, and mudstone of the Upper Permian Longtan Formation, the Changxing-Dalong Formation exposed in the core of the Huijiabao anticline, argillite intercalated with marlstone of the Yelang Formation, and thick bioclastic limestone and dolomite of the Lower Triassic Yongningzhen Formation (Hou et al., 2016). The strata-bound orebodies are mainly on the crest of the anticline and mainly hosted by the Upper Permian Longtan Formation bioclastic limestone. The strata below and above the host rocks are typically thick-bedded argillite, which is

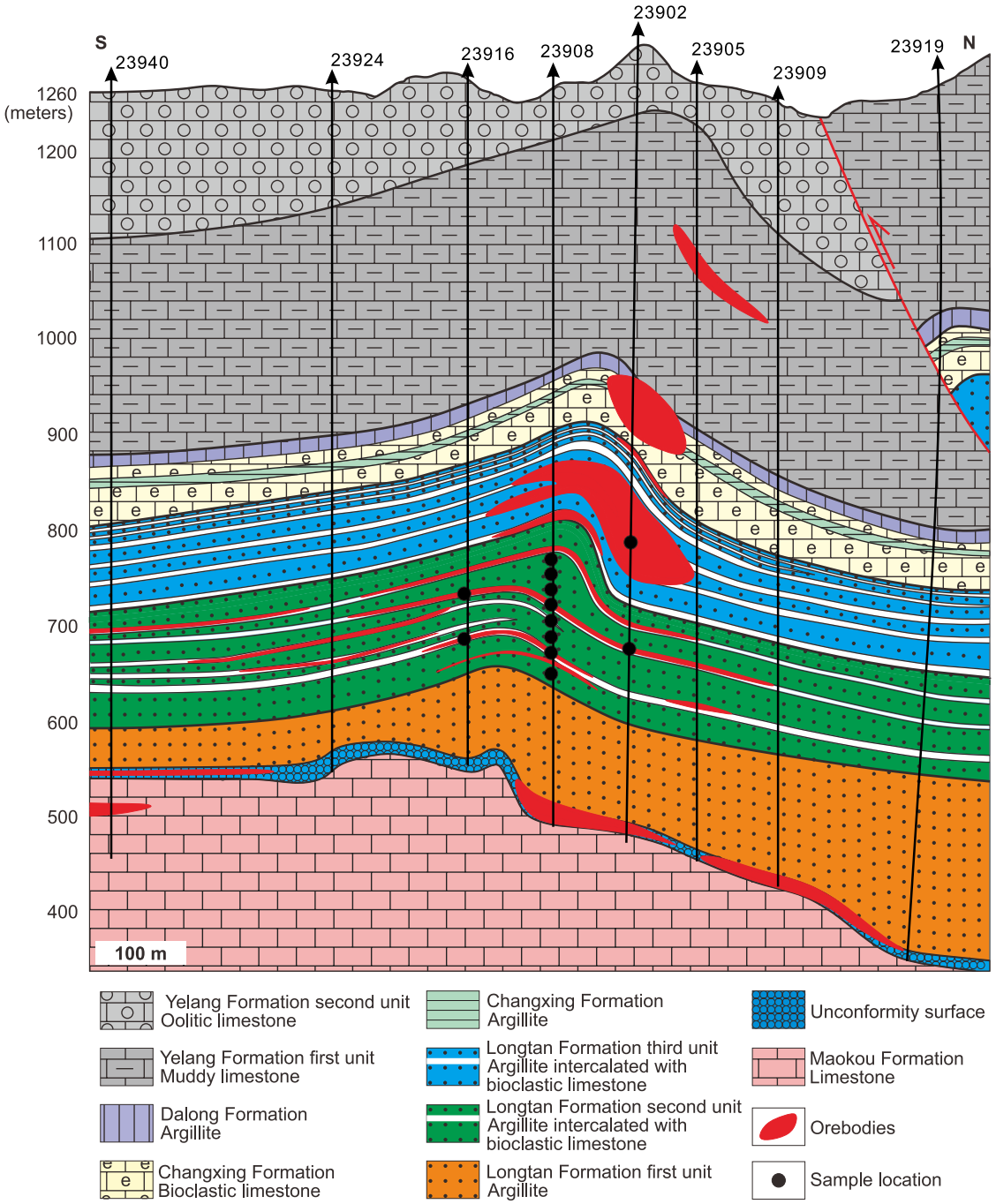

Fig. 2. Deposit geology of the Shuiyindong deposit (adapted from Tan et al., 2015a).

impermeable and may have helped promoting ore fluid reaction with bioclastic limestone. A moderate portion of low-grade strata-bound orebodies, with a proven gold reserve of 69 t (Chen et al., 2019), are hosted by the unconformity between the Longtan Formation and the underlying Maokou Formation, which is previously suggested to be the structural conduit that fed ore fluids into the anticline core (Tan et al., 2015a). Wall rock alteration at Shuiyindong caused decarbonation, silicification, sulfidation and dolomitization. Decarbonation of limestone is confirmed by the occurrence of small relic inclusions of calcite and dolomite in jasperoidal quartz (Su et al., 2009). Sulfides in the deposit consist mainly of arsenian pyrite, arsenopyrite, marcasite and small amounts of orpiment, realgar and stibnite. Gangue minerals include quartz, dolomite, calcite and clay minerals (e.g., illite and kaolinite).

The Lannigou deposit underwent multiple periods of shortening and extension, which are characterized by reactivated faults (F1-F8) (Chen et al., 2011). Gold mineralization is hosted within the faults that truncate Triassic turbidites of the Triassic Xuanman, Niluo, and Bianyang Formations. Several gold orebodies have been discovered at Lannigou, which includes orebodies no. 200, no. 300, no. 503, and no. 506 (Hu

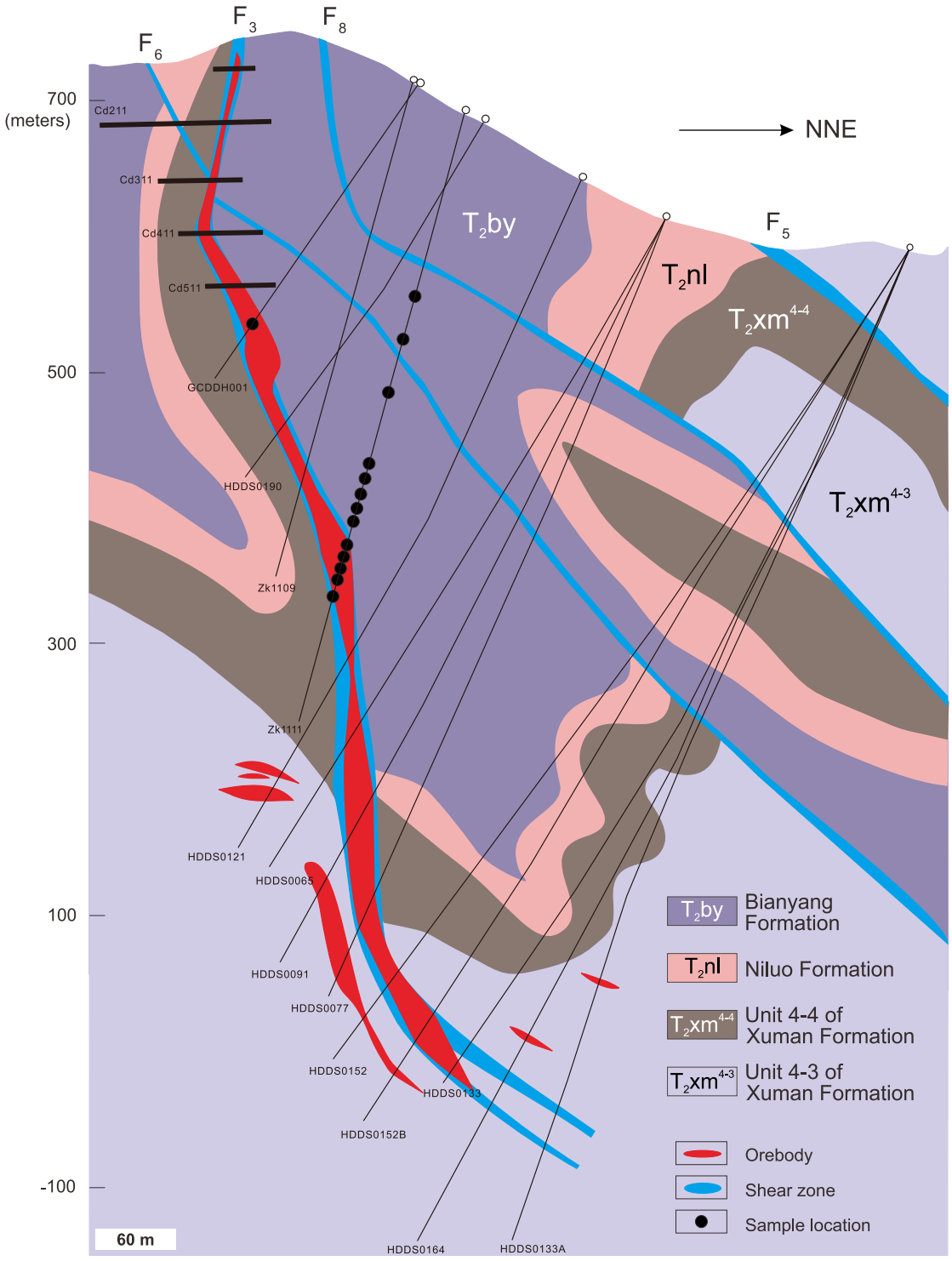

Fig. 3. Deposit geology of the Lannigou deposit (adapted from Xie et al., 2018b).

et al., 2022). The F3 fault zone hosts 80% of Au reserves at Lannigou (Fig. 3). The stratigraphy at Lannigou comprises two main sequences, i.e., the Middle Triassic Xuanman Formation and Bianyang Formation, both of which are main hosts of Au orebodies. The Xuanman Formation is mainly consisted of dolomitic siltstone, thick-bedded to massive calcareous mudstone and sandstone, with a few interlayered sandstone and argillite lenses. The Bianyang Formation lies above the Xuanman Formation and consists largely of Turbiditic sandstone, siltstone and silty argillite, with a total thickness > 300 m. Also present in the deposit is the Middle Triassic Niluo Formation, which is mainly consisted by calcareous claystone. Ore minerals at Lannigou are dominated by pyrite, arsenian pyrite, arsenopyrite, marcasite, realgar, and stibnite, with a small amount of chalcopyrite, sphalerite, and galena. Gangue minerals include quartz, calcite, dolomite, and illite.

In the Shuiyindong and Lannigou deposits, gold mostly occurs as invisible gold (Xie et al., 2018a) in the zoned arsenian pyrite (Fig. 4), which is the main sulfide in the ore stage. No igneous rock has been identified by geologic mapping or drilling in both deposits. The nearest igneous rocks (i.e., the Baiceng alkaline ultramafic dikes, 85–88 Ma, Liu et al., 2010) are ~20 km from Shuiyindong and ~40 km from Lannigou deposit (Fig. 1).

3. Sampling and analytical technique

3.1. Sampling

All the samples were collected from drill cores. A total of 12 samples were collected form the Shuiyindong deposit, and 6 of them are from orebodies and the rest are from wall rocks (Fig. 2). A total of 14 samples were collected from the Lannigou deposit, and 5 of them are from orebodies and the rest are from wall rocks (Fig. 3). The samples were cut into thick sections first, and then the thick sections with ore stage zoned pyrite were etched by NaOCl for 100 s. Typical pre-ore stage pyrite and ore stage pyrite grains with growth bands were selected for sulfur isotope analysis using LA-MC-ICP-MS or SIMS. Elemental mapping and backscattered electron imaging (BSE) analysis were conducted using electron probe microbeam analyzer (EPMA).

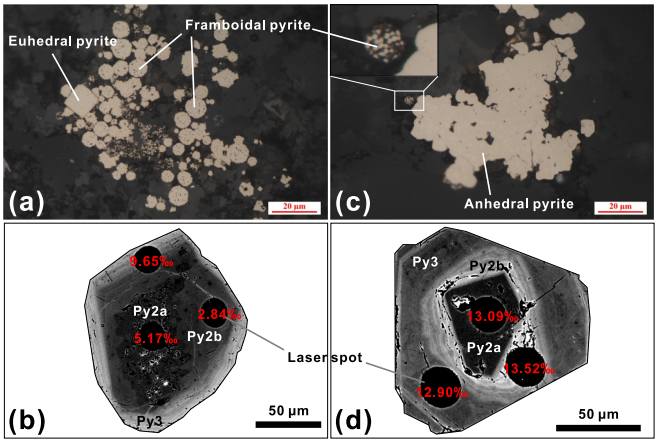

Fig. 4. Photomicrographs of sedimentary pyrite (pre-ore stage, Py1) and ore stage arsenian pyrite (Py2 and Py3) in the Shuiyindong and Lannigou deposits. (a) Plane-polarized light image showing pre-ore stage framboidal pyrite and euhedral pyrite in the host rocks of the Shuiyindong deposit. (b) BSE image showing zoned ore stage pyrite in the Shuiyindong deposit, which is consistent of Py 2a, Py2b and Py3. (c) Plane-polarized light image showing pre-ore stage framboidal pyrite and anhedral pyrite in the host rocks of the Lannigou deposit. (d) BSE image showing zoned ore stage pyrite in the Lannigou deposit, which is consistent of Py 2a, Py2b and Py3. The red numbers in panels b and d are $\delta^{34}S$ values.

3.2. LA-MC-ICP-MS

The LA-MC-ICP-MS analyses were conducted using an ESI NWR193HE ArF excimer (193 nm) laser ablation coupled with the Neptune plus MC-ICP-MS at the State Key Laboratory for Mineral Deposits Research, Nanjing University (Nanjing, China). Argon and ultra-high He were used as auxiliary and carrier gases, and their flow rates were set at 850 and 700 ml/min, respectively. All measurements were in spot mode with a spot size of ~ 15 μm, a repetition rate of 6 Hz and a laser energy of 4 J/cm^2. Each analysis lasted for 60 s, including a 5 s pre-ablation background measurement, 50 s data acquisition and 5 s washout. Cup configuration for sulfur were H3 and C for ^{34}S and ^{32}S, respectively. Mass resolution was set at 4000 to avoid isobaric interference. Instrumental drift and mass bias were corrected using the calibrator-sample bracketing technique, with repeated measurements of reference materials before and after every unknown analysis. Blank was measured every 11 analyses. PPP-1 pyrite ($\delta^{34}S = +5.3 \pm 0.2$‰, 2 SD) (Gilbert et al., 2014) was used for data correction and Py-1 pyrite for quality control ($\delta^{34}S = -0.6 \pm 0.6$‰, 2 SD) (Molnár et al., 2016). The analytical uncertainty, assessed by two times of standard deviation of repeated analysis of the bracketing standards, is mostly better than 1.0‰ (2 SD). The corrected $\delta^{34}S$ value for Py-1 is -0.6 ± 0.7‰ (n = 13, 2 SD), consistent with its recommended value (-0.6 ± 0.6‰, 2 SD; Molnár et al., 2016). The $\delta^{34}S$ values are normalized to the Vienna Canyon Diablo Troilite (V-CDT).

3.3. SIMS

The analysis was conducted using a newly installed Cameca IMS 1300-HR^3 instrument at the State Key Laboratory for Mineral Deposits Research, Nanjing University, China. A primary $^{133}Cs^+$ ion beam (~2nA current and 20 keV total impact energy) was focused on the sample surface. A 10 × 10 μm^2 raster was used in this study and a normal-incidence electron gun was used for charge compensation. An NMR field sensor was applied to stabilize the magnetic field. ^{32}S and ^{34}S were collected simultaneously using two Faraday cups at positions L'2 and H'2, respectively. The L'2 and H'2 positions are configured with 10^{10} Ω and 10^{11} Ω resistor circuits, respectively. The mass resolving power (MRP, M/ΔM), measured at 50% peak height, was set at ~2200 to minimize possible isobaric interferences. The total analytical time was about 4.5 min per pit: 100 s pre-sputtering (to remove the Au coating); ~60 s automatic centering of the secondary ions in the field aperture, and a total of 80 s integration of secondary ions (20 cycles × 4 s). The instrument mass fractionation (IMF) was corrected by repeated analysis of pyrite standard (PPP-1, Gilbert et al., 2014). The data reduction process is as follows.

Instrumental bias correction factors for $\delta^{34}S$ were determined by $\delta^{34}S_{raw}$ of the standards as follows:

$$\alpha_{(SIMS)} = (^{34}S/^{32}S)_{standard\ raw}/(^{34}S/^{32}S)_{standard\ recommend} \quad (1)$$

$$(^{34}S/^{32}S)_{sample} = (^{34}S/^{32}S)_{measured}/\alpha_{(SIMS)} \quad (2)$$

Corrected $^{34}S/^{32}S$ ratios was normalized to the V-CDT according to Equation (3) and taken as true δ-value ($\delta^{34}S$).

$$\delta^{34}S_{sample} = [(^{34}S/^{32}S)_{sample} / (^{34}S/^{32}S)_{V\text{-}CDT} - 1] \times 1000 \quad (3)$$

The analytical uncertainty, assessed by two times of standard deviation of repeated analysis of the standards, is better than 0.3‰ (2 SD).

3.4. EPMA analysis

BSE imaging and elemental mapping were applied to reveal internal texture and chemistry variation of the pyrite grains. All analyses were performed using a JEOL JXA-iSP100 EPMA at the Nanjing Hongchuang Geological Exploration Technology Service Company. The accelerating

voltage for both BSE imaging and elemental mapping is 15 kV. Other parameters include a probe current of 50nA for BSE imaging and 500nA for elemental mapping. The step size for elemental mapping was 0.5 μm, and the dwell time was set to be 200 ms for each step/pixel.

3.5. NaOCl etching

The pyrite grains in this study were etched using commercially available bleach (sodium hypochlorite solution, NaOCl) to reveal internal textures. The thick section with pyrite were immersed into NaOCl solution for 90 to 120 s, until a noticeable color change of the pyrite occurred. The samples were then rinsed with cold water and allowed to dry. The tarnishing mostly occurs during drying. The NaOCl act as an oxidant for the pyrite, and the discoloration patches and zones reflect compositional differences within the pyrite grains (Sykora et al., 2018).

4. Results

4.1. Pyrite texture and EPMA analysis results

The pyrite in Shuiyindong deposit can be divided into three stages (i.e., Py1, Py2 and Py3) according to petrographic observation, BSE imaging and NaOCl etching (Figs. 4, 5). Framboidal and euhedral pyrites were assigned to Py1 (Fig. 4a). Py2 are zoned pyrite grains, which generally consist of porous core (Py2a) and compact mantle (Py2b) (Fig. 4b). Py2b is rimed by Py3 (Fig. 4b). In BSE images, the luminance decreases from Py2a to Py3, and the contact boundary of Py2a and Py2b are generally ragged (Fig. 4b). The different bands in BSE images are the same as that shown in pyrite grains (Py2 and Py3) after NaOCl etching (Fig. 5). The As concentration increases from Py2a to Py3 (Fig. 5). Au concentration is low in Py2a and Py2b and high in Py3 (Fig. 5).

Similar to Shuiyindong deposit, the pyrite at Lannigou can also be divided into Py1, Py2a, Py2b and Py3. Framboidal and anhedral pyrites were assigned to Py1 (Fig. 4c). Py2a and Py2b have the lowest and highest luminance in BSE image, respectively, while Py3 has luminance intermediate to Py2a and Py2b (Fig. 4d). The color of Py2a only changed a little after NaOCl etching compared with its original color (Fig. 6). Py2b is indigo and Py3 is orange-yellow (Fig. 6). The contact boundaries between Py2a, Py2b and Py3 are straight in most cases (Fig. 4d). We observed ubiquitous cracks at the boundary of Py2a and Py2b (Fig. 6). Py2a is As- and Au-poor, Py2b is As-rich and Au-poor, while Py3 is As-poor and Au-rich (Fig. 6).

4.2. LA-MC-ICP-MS and SIMS analysis

The $\delta^{34}S$ values of Py1 in Shuiyindong deposit range from −41.40 to +34.17‰ (average at −18.37 ± 33.99‰, 2SD, n = 113) (Fig. 7a, see Supplementary material 1 for detail). The $\delta^{34}S$ ranges from +5.17 to +14.77‰ (average at +10.15‰ ± 4.89‰, 2SD, n = 38) for Py2a, from +2.84 to +10.58‰ (average at +6.08‰ ± 5.14‰, 2SD, n = 22) for Py2b and from +3.57 to +13.01‰ (average at +6.44‰ ± 3.97‰, 2SD, n = 58) for Py3. For the Lannigou deposit, $\delta^{34}S$ values range from −53.30 to +19.80‰ (average at −21.90 ± 29.66‰, 2SD, n = 110) for Py1 (Fig. 7b, see Supplementary material 1 for detail), from +5.17 to +13.84‰ (average at +12.36 ± 2.81‰, 2SD, n = 43) for Py2a, from +11.08 to +13.97‰ (average at +13.05‰ ± 1.42‰, 2SD, n = 42) for Py2b and from +11.04 to +14.33‰ (average at +12.91‰ ± 1.37‰, 2SD, n = 44) for Py3. No obvious difference is observed between LA-MC-ICP-MS and SIMS results. More details about the results are given in the supplementary material 1.

The Py1 in the wall rocks (Fig. 4), whose sulfur isotopic composition is highly variable (Fig. 7a, b), is assigned to pre-ore stage. The Py2 and Py3, which generally have elevated As and Au concentration (Figs. 5, 6) and narrow sulfur isotope range (Fig. 7), are assigned to ore stage.

5. Discussion

5.1. A non-magmatic origin for the ore-forming fluids

The sulfur isotope data of pre-ore pyrite in the wall rocks at Shuiyindong and Lannigou is presented in Fig. 7a and b, and the sulfur isotope data of ore stage pyrite from Shuiyindong and Lannigou deposits is shown in Fig. 7c and 7d, respectively. The sulfur isotope of ore stage pyrite is plotted together with the data from published literatures for comparison (Fig. 7e; see Supplementary material 1 for detail). Since sedimentary and Au-bearing pyrite could occur in one grain in the orebodies hosted in sedimentary rocks, only in-situ sulfur isotope results are used here. Some orebodies are hosted in diabase in the Zhesang, Anna and Badu deposits, in which the pyrite grains are free from contamination of sedimentary pyrite, and their bulk sulfur isotope analyses are also incorporated into Fig. 7e.

The $\delta^{34}S$ values of ore stage pyrite at the Shuiyindong deposit cluster

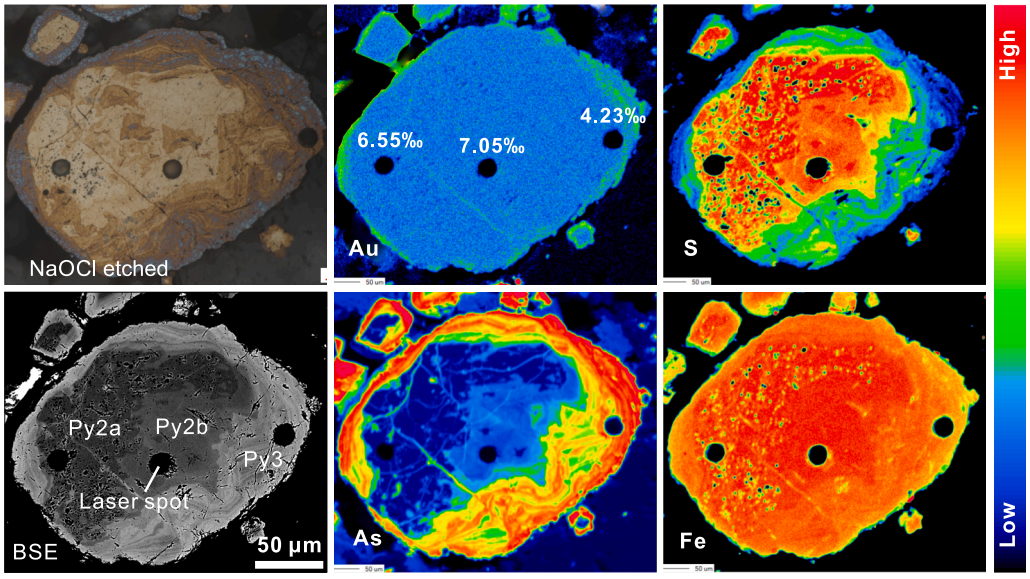

Fig. 5. Photomicrograph, BSE imaging and element mapping of Py2 and Py3 in the Shuiyindong deposit. The numbers are the sulfur isotope composition of analyzed pyrite.

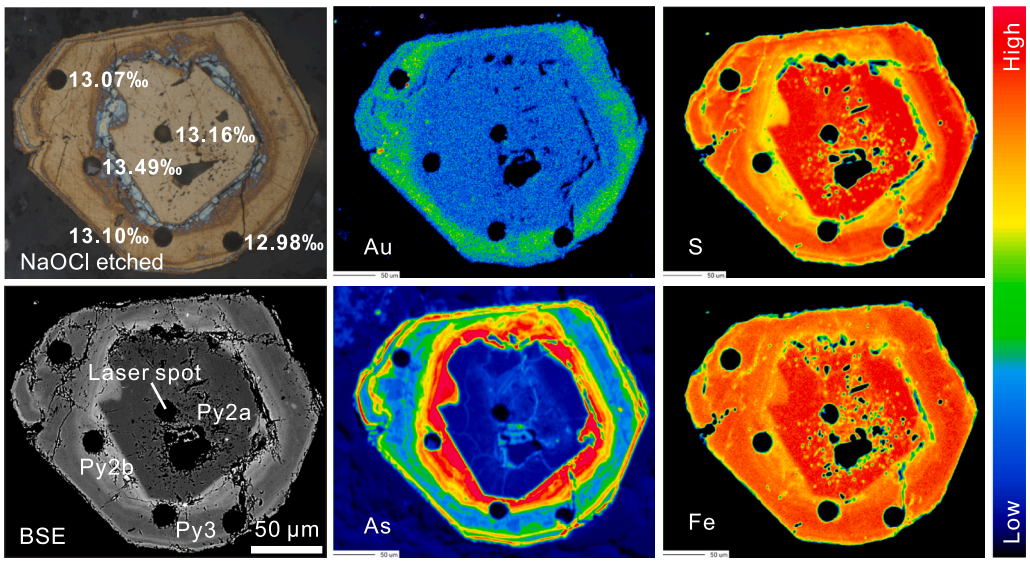

Fig. 6. Photomicrograph, BSE imaging and element mapping of Py2 and Py3 in the Lannigou deposit. The numbers are the sulfur isotope composition of analyzed pyrite.

in the range of +3 to +10‰ and average at +6.11‰, while they cluster in the range of +11 to +14‰ and average at +13.16‰ at the Lannigou deposit (Fig. 7c-d). When all the deposits in the "Golden Triangle" area are considered together, the variation of the $\delta^{34}S$ values of Au-bearing pyrite can reach up to 27.5‰ (i.e., from − 7.5 to +20‰) (Fig. 7c-e). Given that ore-stage minerals are mainly sulfides (e.g., pyrite, arsenopyrite) (Lin et al., 2021; Su et al., 2018; Xie et al., 2018a) and CH_4 is present in the fluid inclusions (Su et al., 2009), the fugacity of the ore-forming fluids should be low. Based on fluid inclusion studies, the temperature of the ore-forming fluids is in the range of 200–300 °C (Su et al., 2018). In this context, the variation of $\delta^{34}S_{pyrite}$ caused by fluctuation in temperature and oxygen fugacity should be in the range of 0 to 3.1‰ (Fig. 8). Assuming a magmatic sulfur for the ore-forming fluids (−5 to +5‰; Seal, 2006), the pyrite precipitated from them should have $\delta^{34}S$ values in the range of −8 to +5‰. This range is much narrower than the observed Au-bearing pyrite in this study (−7.5 to +20‰), which precludes a dominant magmatic source for the ore-forming fluids.

Co/Ni ratio has long been used to trace the formation environment of pyrite (e.g., Bralia et al., 1979), and it serves as a powerful tool in discriminating sedimentary and magma-related hydrthermal pyrite (e.g., Large et al., 2014; Li et al., 2020b; Ulrich et al., 2011). Here we compiled published Co and Ni data of pyrite from both sedimentary and magmatic-hydrothermal environments (see supplementary material 2 for detail). The available dataset shows that the pyrites in sedimentary rocks generally have Co/Ni < 2 (Large et al., 2014), while those in magmatic-hydrothermal deposits have much wider range (e.g., 10^{-4} to 10^{3}) (e.g., Li et al., 2018; Zhang et al., 2016) (Fig. 9) and the variation of Co/Ni is frenquently reported to vary across 4 orders of magnitude for magmatic-hydrothermal deposits (e.g., Li et al., 2018). The Co/Ni ratios of sedimentary pyrite in the host rocks and Au-bearing pyrite in the "Golden Triangle" area are generally consistent with each other, with most data showing Co/Ni < 2 (Fig. 9), in sharp contrast with the pyrite that formed in magma-related hydrothermal environment. This indicates that the Co and Ni in ore stage pyrite of the study area are of sedimentary origin rather than magmatic origin.

The available geochronology results of mineralization and magmatism in the area also preclude a strong correlation with magmatic fluids. The compilation of U-Pb dating of calcite and other dating results indicate two metallogenic episodes in this area, i.e., the Late Triassic episod (~200 Ma) and the Early Cretaceous episode (~140 Ma) (Gao et al., 2021; Jin et al., 2021; Pi et al., 2017), and the Au mineralization occurred mostly in the former episode (e.g., Shuiyindong, Lannigou, Laizishan, Yata, Jinya, Banqi, Laozhaiwan, Zhesang). The interspersed igneous rocks in the "Golden Triangle" area are much younger than any of aforementioned metallogenic episodes (Fig. 1). For example, the Baiceng alkaline ultramafic dike, which is the nearest igneous rock to Shuiyindong and Lannigou, has an age of ca. 88–85 Ma; the quartz porphyry dikes occurring in the east of this area have an emplacement age of ca. 97–95 Ma; the granite intrusions in the south, east and northeast of this area generally have ages around ca. 96–80 Ma (Xie et al., 2018b and references therein). Besides, the Au mineralization doesn't occur spatially around these igneous rocks, which furtherly precludes a magmatic fluid source. This conclusion is further supported by the latest seismic data which suggests that there is no deep-seated magmatic plutons/batholiths in this area (Hu et al., 2022).

5.2. Potential source of the ore-forming materials

As mentioned above, the combination of available sulfur isotope, trace element and geochronology data does not support a magmatic origin for the ore-forming materials in the study area. Rather, the wide $\delta^{34}S$ range and the low Co/Ni ratios (<2) of Au-bearing pyrite seem to support a sedimentary origin.

It should be noted that the ore-forming materials are not likely sourced directly from the ore-hosting sedimentary rocks. To evaluate the potential contribution of sulfur from ore-hosting sedimentary rocks, the sulfur isotopic compositions of pre-ore pyrite in the ore-hosting sedimentary rocks should be determined. Some in-situ sulfur isotopic data of pre-ore pyrite in the study area have been reported in recent years (e.g., Hou et al., 2016), but the data set is relatively small so that the results could deviate from the average $\delta^{34}S$ value of pre-ore pyrite. This is because there are different types of pyrite (e.g., framboidal / euhedral / anhedral pyrite) in the sedimentary rocks, and they could be distinct in their sulfur isotopic compositions (e.g., Lin et al., 2016). In this study, we analyzed all types of the pyrite grains (Fig. 4a, c) that are presenting in the thick sections and large enough for SIMS analysis. The average $\delta^{34}S$ value of pre-ore stage pyrite in Shuiyindong and Lannigou are −18.37‰ (n = 113) and −21.90‰ (n = 110), respectively (Fig. 7). These results are generally consistent with the reported $\delta^{34}S$ values of Late Permian to Early Triassic sedimentary rocks from South China using the chromium reduction method (e.g., average at −25‰; Shen et al., 2011), indicating that the results of this study are representative of pre-ore pyrite. Given that the pre-ore pyrite in the study area has $\delta^{34}S$ values around −21.90 to −18.37‰, the $\delta^{34}S$ of the ore-forming fluid is much

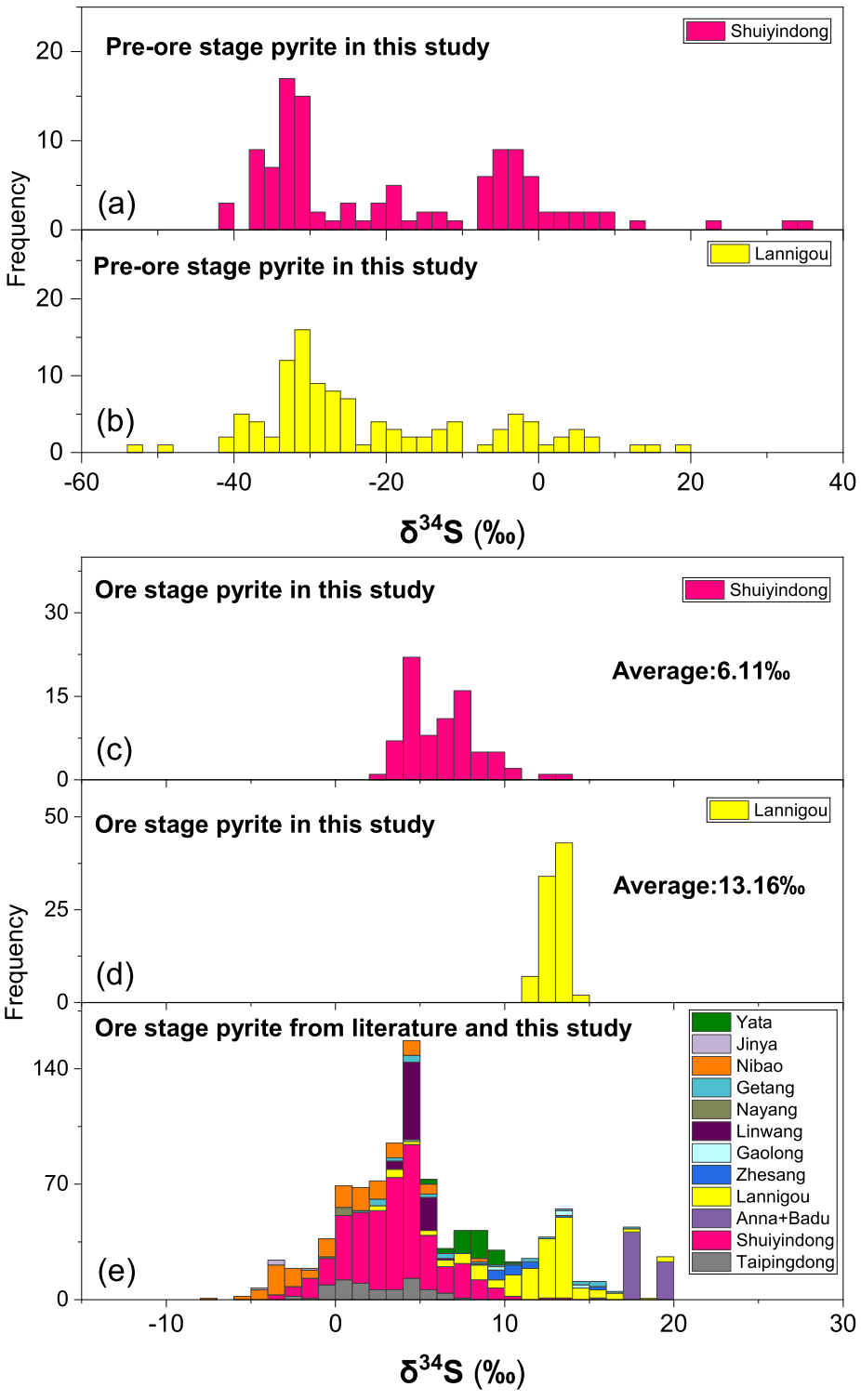

Fig. 7. Sulfur isotopic composition of pyrite in the "Golden Triangle" area. (a) Sulfur isotopic composition of pre-ore pyrite at the Shuiyindong deposit. (b) Sulfur isotopic composition of pre-ore pyrite at the Lannigou deposit. (c) Sulfur isotopic composition of ore stage pyrite at the Shuiyindong deposit. (d) Sulfur isotopic composition of ore stage pyrite at the Lannigou deposit. (e) Compiled in-situ sulfur isotope data of Au-bearing pyrite from this study and literatures. Data sources include: (Dai et al., 2014, He et al., 2021, Hou et al., 2016, Hu et al., 2018, Jin, 2017, Li et al., 2020a, Li et al., 2019, Liang et al., 2020, Lin et al., 2021, Liu, 2019, Su et al., 2018, Xie et al., 2018b, Yan et al., 2018, Zhang et al., 2017, Zhang et al., 2013, Zhao et al., 2020, Zheng et al., 2019). Bulk analyses of Zhesang, Anna and Badu are compiled into this figure given that the orebodies hosted in the diabase should have no contamination from sedimentary pyrite (Su et al., 2018).

higher than that of pre-ore pyrite in the host rocks, preventing them as major fluid source.

Recently, Yang et al. (2022) did new in-situ sulfur isotope analysis of sedimentary and ore stage pyrite, and compiled reported sulfur isotope data from the "Golden Triangle" area, from which they found that the sulfur isotopic composition of ore stage pyrite is correlated with sedimentary pyrite and concluded that the sulfur in the ore stage pyrite is sourced from sedimentary pyrite. We note that the sulfur isotopic composition of the sedimentary host rocks in Yang et al. (2022) is mostly positive, and this is not consistent with reported sulfur isotopic composition of global Permian and Triassic sedimentary pyrite (Canfield and Farquhar, 2009). Generally, the magnitude of sulfur isotope fractionation ($\Delta^{34}S_{sulfate\text{-}sulfide}$) is negatively correlated with the rate of sulfate reduction (Canfield, 2001), and the rate of sulfate reduction is positively correlated with the concentration of organic material (Westrich and Berner, 1984). This means that lower organic material would result in an increased sulfur isotope fractionation, and consequently lower sulfur isotopic composition of sulfides. So, the sulfides in the open basin tends to have low $\delta^{34}S$ values (generally having $\delta^{34}S < 0$ ‰) (e.g., Fike et al., 2015), a phenomenon that is not observed in Yang et al.

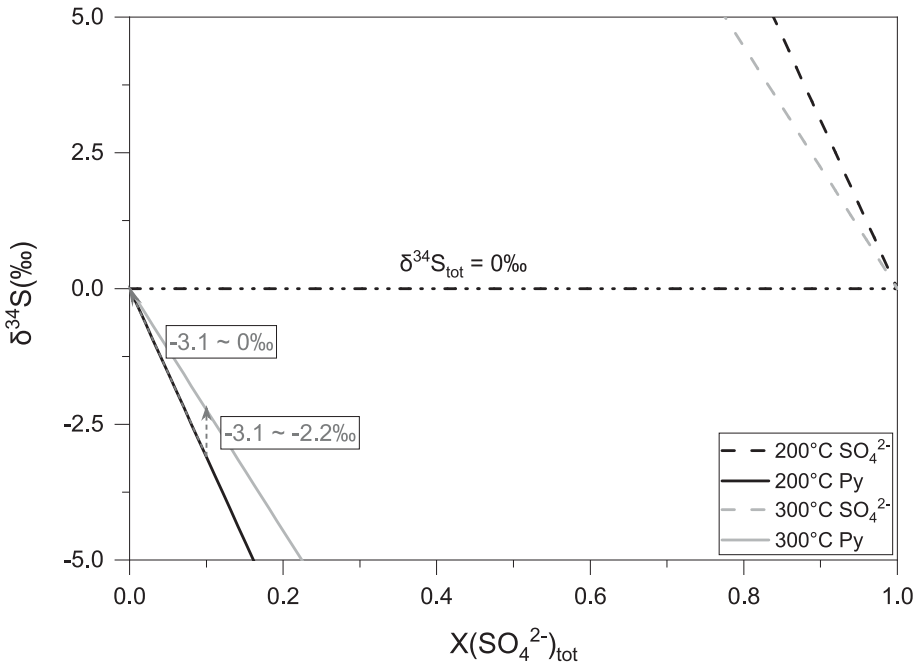

Fig. 8. Modeled $\delta^{34}S$ values of the Au-bearing pyrite at the "Golden Triangle" area. The temperature of ore-forming fluid is adapted from Su et al. (2018) and the fractionation factor (α) is taken from Sakai (1968). The fugacity of the ore-forming fluid is estimated to be low since the major mineral is sulfide minerals (e.g., pyrite and arsenopyrite) and CH_4 is present in fluid inclusions (Su et al., 2009).

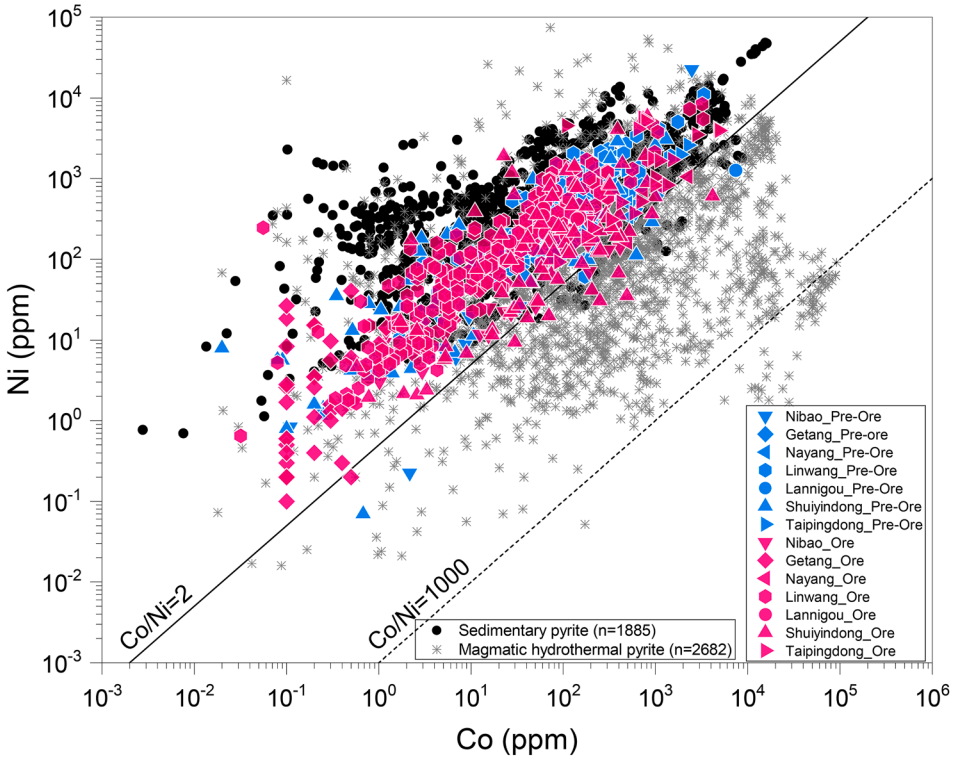

Fig. 9. Co vs Ni plot of pre-ore and ore-stage pyrite from the "Golden Triangle" area. The data of sedimentary (Large et al., 2014) and magmatic-hydrothermal pyrite worldwide (Chen et al., 2020, Du et al., 2020, Keith et al., 2016, Li et al., 2018, Li et al., 2017, Liang et al., 2021, Wang et al., 2017, Wang et al., 2015, Zhang et al., 2016) are also shown for comparison. The Co/Ni ratios of ore-stage pyrite in the "Golden Triangle" are mostly < 2 (Hou et al., 2016, Hu et al., 2018, Li et al., 2020a, Li et al., 2019, Wei et al., 2020, Xie et al., 2018b), resembling typical sedimentary pyrite worldwide, which indicates a major contribution of metals (e.g., Co and Ni) from regional metasedimentary rocks.

(2022). Consequently, more results are needed confirm the sulfur isotopic composition of sedimentary pyrite, and the relationship between sedimentary pyrite and ore stage pyrite needs reconsideration. Additionally, if we assume that the sulfur in ore stage pyrite comes from sedimentary host rocks, it is difficult to explain the large sulfur isotope difference between sedimentary pyrite and ore stage pyrite in some deposits. For example, at Lianhuashan deposit, the reported $\delta^{34}S$ for sedimentary pyrite is around −11.5‰, and for the ore pyrite is around +0.5‰ (Yang et al., 2022). At Badu deposit, the $\delta^{34}S$ for sedimentary pyrite is around −20‰, and for the ore pyrite hosted in the sedimentary wall rock is around +17‰ (Wei et al., 2022). Other examples come from this study, i.e., Shuiyindong and Lannigou (Fig. 7). For the reasons listed above, we think that the sedimentary host rocks may not be the major source for the sulfur in the ore stage pyrite.

Basinal fluid is not a possible candidate neither. The sedimentary rocks in the area are marine facies before Middle Triassic and turned to terrestrial facies from Late Triassic to Neogene (Chen, 2010). The common absence of Late Triassic marine facies sedimentary rocks in this area indicates that the closure of the Youjiang basin should not be later than the Carnian (i.e., > 230 Ma) (Lehrmann et al., 2015; Wang et al., 1995). Therefore, the closure of the basin is at least 30 Myr earlier than the formation of the gold deposits, which argues against major contribution of basin fluids to the ore-forming fluids. Additional evidence comes from sulfur isotope data. Assuming there is remnant seawater in the Youjiang basin at ~200 Ma, and the $\delta^{34}S$ values of the seawater is around +15‰ (Wu et al., 2010). To offer sulfur for the ore-forming fluids, the seawater should be reduced. Bacterial sulfate reduction would result in H_2S at around −25‰ (e.g., Jin, 2017; Shen et al., 2011), which is much lower than the ore-forming fluids. Thermochemical sulfate reduction would result in an offset of sulfur isotope about 15‰ (Ohmoto and Goldhaber, 1997), resulting H_2S with $\delta^{34}S$ values at around 0‰. This scenario cannot reconcile with the fact that most Au-bearing pyrite in the "Golden Triangle" area have $\delta^{34}S$ values > 0‰ (Fig. 7e). The latest Mg isotope results indicate that ore stage dolomite has $\delta^{26}Mg$ values ranging from −3.49 to −0.07‰, which is significantly heavier than that of normal carbonate rocks, indicating that the gold deposits in this area were not formed from shallow ore fluids (e.g., meteoric water or basin fluid) (Xie et al., 2022). The Mg isotope result provides further support for the conclusion that the ore-forming fluid couldn't be sourced from basinal fluids.

The variable $\delta^{34}S$ values of Au-bearing pyrite in the "Golden Triangle" area resemble that reported for orogenic deposit worldwide, which is suggested to have sourced from metamorphism of sedimentary rocks (Goldfarb and Groves, 2015). Similarly, we suggest that the ore-forming materials in the study area are also sourced from deep buried metasedimentary rocks. According to the sulfur isotope record worldwide and South China, we find that the sedimentary rocks in the Phanerozoic generally have negative $\delta^{34}S$ values, while those older than 500 Ma tend to have positive $\delta^{34}S$ values (Fig. 10) (Canfield and Farquhar, 2009; Cui et al., 2016; Cui et al., 2018; Farquhar et al., 2010; Lin et al., 2020). The strata older than 500 Ma are widespread in the study area (Chen, 2010; Cui et al., 2016; Shu et al., 2021; Su et al., 2018), and metamorphism of these strata would release sulfur with positive $\delta^{34}S$ values covering what was observed in the Au-bearing pyrite. Independent H-O isotope studies also support a metamorphosed sedimentary origin for the ore-forming fluids (Hofstra et al., 2005; Su et al., 2018).

Recent studies have revealed that initial collision and amalgamation of the Qamdo-Simao terrane (Indochina) with the Yangtze Block (South China) along the Jinshajiang-Ailaoshan and Song Ma sutures took place at the Early Triassic (254–237 Ma) (Zi et al., 2012). Further studies suggested that the Ailaoshan tectonic zone had evolved into a post-collisional setting by the Late Triassic (ca. 230–200 Ma) (Liu et al., 2014; Liu et al., 2012). This means that the gold deposits in the "Golden Triangle" area were formed at the wanning stage of continental collision, during which the metamorphism of old sedimentary rocks (>500 Ma) may have facilitated generation of the ore-forming fluids responsible for the gold deposits.

It is widely accepted that elements like Au, As, Co, Ni, Ag, Cu, Zn, Mo and Pb could be initially enriched in the sedimentary pyrite and organic matter (Hu et al., 2016), and could be liberated during diagenesis and metamorphism (Large et al., 2011). Recent studies revealed that these trace elements can be effectively liberated at much lower metamorphic temperatures than that of the pyrite-pyrrhotite transition (Wu et al., 2020), which means that except for sulfur, low-grade metamorphism of sedimentary rocks > 500 Ma may have also released Au, Co and Ni into the ore-forming fluids. The Au concentration data of the metasedimentary rocks > 500 Ma are scarce, but reported data for some Early Cambrian black shales have an average value of 8.21 ppb (n = 22) (Xu et al., 2013 and references therein), significantly higher than that of upper crust (1.8 ppb) (McLennan, 2001), which is a candidate source for the Au mineralization in the "Golden Triangle" area.

Previous study by Su et al. (2009) indicates that the ore-forming fluids are Fe-poor, and the Fe in Au-bearing pyrite are possibly derived from dissolution of ferroan minerals in the host rocks. One may expect that the Co and Ni in the Au-bearing pyrite are also derived from sedimentary wall rocks, which resulted a Co/Ni < 2 for the Au-bearing pyrite. However, we think that Fe in Au-bearing pyrite was derived from ferroan minerals in the host rocks doesn't necessarily mean that the Co and Ni in gold-bearing pyrite are also sourced from host rocks. An example to elucidate this is from the Badu deposit. There are two types of host rocks at Badu deposit, i.e., sedimentary rocks and diabase (Wei et al., 2022). It is suggested that the ore pyrite hosted in the sedimentary rocks (Py3a) is formed through sulfidation of Fe-carbonates, while those hosted in the diabase (Py3b) is formed through sulfidation of Fe-bearing minerals like clinopyroxene and ilmenite (Wei et al., 2022). If Co and Ni have the same source with that of Fe, then the ore pyrite (Py3) should have Co/Ni ratios similar to that of the source rocks. However, both types of ore pyrite in the sedimentary rocks and the diabase have Co/Ni ratios mostly < 1 (Wei et al., 2022). This is not consistent with the hypothesis that the Co and Ni in ore pyrite hosted in the diabase are sourced from the diabase, which generally has a Co/Ni range from 0.01 to 50 (Fig. S1, Supplementary material 3). Alternatively, we suggest that

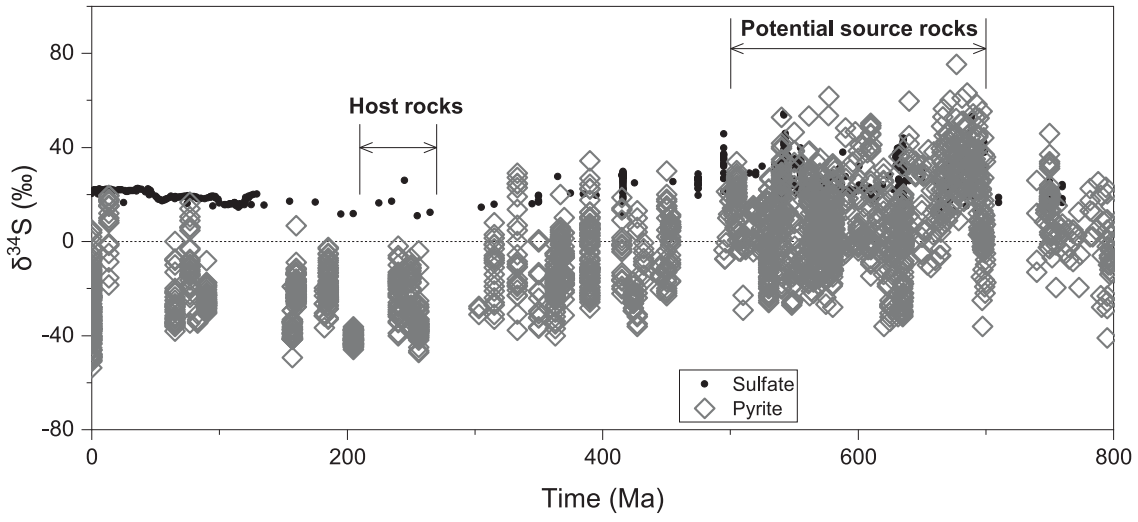

Fig. 10. Sulfate and pyrite sulfur isotope data of sedimentary pyrite in the past 800 Myr (Canfield and Farquhar, 2009, Cui et al., 2016).

the consistently low Co/Ni ratios in the ore stage pyrite indicates a uniform source for Co and Ni in the ore-forming fluid, i.e., the fluids released by metamorphism of old sedimentary rocks (>500 Ma) in the studied area.

6. Conclusions

In-situ elemental and isotopic analyses of the Au-bearing pyrite in the "Golden Triangle" area reveal a wide range of $\delta^{34}S$ values (−7.5 to +20‰) and consistent low Co/Ni ratios (mostly < 2), which argue against magmatic fluids as a major contributor for the ore-forming fluids in this area. In contrast, the data present solid evidence for a metasedimentary origin for the Au-bearing ore-forming fluids. Based on the comparison of sulfur isotopes, we suggest that the Au-bearing ore-forming fluids may have eventually sourced from the >500 Ma metasedimentary rocks in the study area. The late Triassic regional metamorphism of the Early Cambrian black shales during the closure of the Paleo-Tethys may have released S, Au, Co and Ni into the ore-forming fluids.

Declaration of Competing Interest

The authors declare that they have no known competing financial interests or personal relationships that could have appeared to influence the work reported in this paper.

Data availability

I have shared the data with the link to the supplementary files.

Acknowledgements

This study is supported by the National Natural Science Foundation of China (42273010, 42103058). We thank Dr. Haoran Dou for his assistance during EPMA analysis. We appreciate the thoughtful comments from three anonymous reviewers.

Appendix A. Supplementary data

Supplementary data to this article can be found online at https://doi.org/10.1016/j.oregeorev.2023.105560.

References

Bralia, A., Sabatini, G., Troja, F., 1979. A revaluation of the Co/Ni ratio in pyrite as geochemical tool in ore genesis problems. Mineral. Deposita. 14, 353–374.
Canfield, D.E., 2001. Isotope fractionation by natural populations of sulfate-reducing bacteria. Geochim. Cosmochim. Acta 65 (7), 1117–1124.
Canfield, D.E., Farquhar, J., 2009. Animal evolution, bioturbation, and the sulfate concentration of the oceans. PNAS 106 (20), 8123–8127.
Chen, L., 2010. Rhenium-Osmium Isotopic Features Of Bitumen From the Majiang Marine Paleo-Oil Reservoir in South China: Constraints for Timing Of Hydrocarbon Accumulation And Reservoir Destruction. China University of Geosciences (Wuhan).
Chen, F., Deng, J., Wang, Q., Huizenga, J.M., Li, G., Gu, Y., 2020. LA-ICP-MS trace element analysis of magnetite and pyrite from the Hetaoping Fe-Zn-Pb skarn deposit in Baoshan block, SW China: Implications for ore-forming processes. Ore Geol. Rev. 117, 103309.
Chen, F.-e., Liu, J.-z., Yang, C.-f., Liu, Y., Zhang, Z.-x., Wang, Z.-p., et al., 2019. Geological characteristics and structural ore control analysis of Shu-iyindong super large gold deposit in Zhenfeng County, Guizhou Province. Guizhou Geol. 36, 18–27.
Cline, J., Hofstra, A., Muntean, J., Tosdal, R., Hickey, K., 2005. Carlin-type gold deposits in Nevada: Critical geologic characteristics and viable models. Econ. Geol. 100th Anniv. Vol. 451–484.
Cline, J., Muntean, J.L., Gu, X., Xia, Y., 2013. A comparison of Carlin-type gold deposits: Guizhou Province, golden triangle, southwest China, and northern Nevada, USA. Earth Sci. Front. 20, 1–18.
Cui, H., Kaufman, A.J., Xiao, S., Peek, S., Cao, H., Min, X., Cai, Y., Siegel, Z., Liu, X.-M., Peng, Y., Schiffbauer, J.D., Martin, A.J., 2016. Environmental context for the terminal Ediacaran biomineralization of animals. Geobiology 14 (4), 344–363.
Cui, H., Kitajima, K., Spicuzza, M.J., Fournelle, J.H., Denny, A., Ishida, A., Zhang, F., Valley, J.W., 2018. Questioning the biogenicity of Neoproterozoic superheavy pyrite by SIMS. Am. Mineral. 103 (9), 1362–1400.
Dai, H., Chen, C., Gu, X., Li, B., Dang, S., Cheng, W., 2014. Typomorphic characteristics of gold-bearing minerals in Zhesang gold deposit, Yunnan Province. Mineral Deposit. 33, 70–86.
Dong, W., Su, W., Shen, N., Zhu, L., Cai, J., 2017. Mineralogy and geochemistry of gold-bearing sulfides in Badu gold deposit, Guangxi Province. Acta Mineral. Sinca. 37, 16–28.
Du, H., Zheng, J., Tian, L., Liang, H., Guo, J., Li, Y., 2020. Microfabrics, in-situ trace element and sulfur isotope compositions of pyrite from the Jinjiwo copper deposit in Chengmenshan orefield, northern Yangtze Block: Syngenetic stratabound mineralization and hydrothermal remobilization. Ore Geol. Rev. 127, 103830.
Farquhar, J., Wu, N., Canfield, D.E., Oduro, H., 2010. Connections between sulfur cycle evolution, sulfur isotopes, sediments, and base metal sulfide deposits. Econ. Geol. 105 (3), 509–533.
Fike, D.A., Bradley, A.S., Rose, C.V., 2015. Rethinking the ancient sulfur cycle. Annu. Rev. Earth Planet. Sci. 43 (1), 593–622.
Gao, W., Hu, R., Hofstra, A.H., Li, Q., Zhu, J., Peng, K., et al., 2021. U-Pb dating on hydrothermal rutile and monazite from the badu gold deposit supports an early cretaceous age for carlin-type gold mineralization in the Youjiang Basin, Southwestern China. Econ. Geol. 116, 1355–1385.
Gilbert, S.E., Danyushevsky, L.V., Rodemann, T., Shimizu, N., Gurenko, A., Meffre, S., Thomas, H., Large, R.R., Death, D., 2014. Optimisation of laser parameters for the analysis of sulphur isotopes in sulphide minerals by laser ablation ICP-MS. J. Anal. At. Spectrom 29 (6), 1042–1051.
Goldfarb, R.J., Groves, D.I., 2015. Orogenic gold: Common or evolving fluid and metal sources through time. Lithos 233, 2–26.
He, X., Su, W., Shen, N., Xia, X., Wang, F., 2021. In situ multiple sulfur isotopes and trace element compositions of pyrite support a sedimentary source-rock model for Linwang Carlin-type gold deposit in the Youjiang basin, Southwest China. Ore Geol. Rev., 104533
Hofstra, A.H., Emsbo, P., Christiansen, W.D., Theodorakos, P., Zhang, X.-C., Hu, R.-Z., et al., 2005. Source of ore fluids in Carlin-type gold deposits, China: Implications for genetic models. Springer Berlin Heidelberg, Berlin, Heidelberg, pp. 533–536.
Hou, L., Peng, H., Ding, J., Zhang, J., Zhu, S., Wu, S., Wu, Y., Ouyang, H., 2016. Textures and in situ chemical and isotopic analyses of Pyrite, Huijiabao Trend, Youjiang Basin, China: Implications for Paragenesis and Source of Sulfur. Econ. Geol. 111 (2), 331–353.
Hu, S.-Y., Evans, K., Fisher, L., Rempel, K., Craw, D., Evans, N.J., Cumberland, S., Robert, A., Grice, K., 2016. Associations between sulfides, carbonaceous material, gold and other trace elements in polyframboids: Implications for the source of orogenic gold deposits, Otago Schist, New Zealand. Geochim. Cosmochim. Acta 180, 197–213.
Hu, X., Gong, Y., Zeng, G., Zhang, Z., Wang, J., Yao, S., 2018. Multistage pyrite in the Getang sediment-hosted disseminated gold deposit, southwestern Guizhou Province, China: Insights from textures and in situ chemical and sulfur isotopic analyses. Ore Geol. Rev. 99, 1–16.
Hu, Y., Liu, W., Zhang, G., Guan, S., Lu, Y., Li, P., et al., 2022. Seismic reflection profiles reveal the ore-controlling structures of carlin-style gold deposits in Lannigou Gold Fields, Southwestern Guizhou. China. Econ. Geol. 117, 1203–1224.
Jin, X.-Y., 2017. Geology, Mineralization And Genesis of the Nibao, Shuiyindong and Yata Gold Deposits in SW Guizhou Province. China University of Geosciences (Wuhan), China.
Jin, X.-Y., Zhao, J.-X., Feng, Y.-X., Hofstra, A.H., Deng, X.-D., Zhao, X.-F., et al., 2021. Calcite U-Pb dating unravels the age and hydrothermal history of the giant Shuiyindong Carlin-type gold deposit in the Golden Triangle, South China. Econ. Geol. 116, 1253–1265.
Keith, M., Haase, K.M., Klemd, R., Krumm, S., Strauss, H., 2016. Systematic variations of trace element and sulfur isotope compositions in pyrite with stratigraphic depth in the Skouriotissa volcanic-hosted massive sulfide deposit, Troodos ophiolite, Cyprus. Chem. Geol. 423, 7–18.
Large, R.R., Bull, S.W., Maslennikov, V.V., 2011. A carbonaceous sedimentary source-rock model for carlin-type and orogenic gold deposits. Econ. Geol. 106 (3), 331–358.
Large, R.R., Halpin, J.A., Danyushevsky, L.V., Maslennikov, V.V., Bull, S.W., Long, J.A., Gregory, D.D., Lounejeva, E., Lyons, T.W., Sack, P.J., McGoldrick, P.J., Calver, C.R., 2014. Trace element content of sedimentary pyrite as a new proxy for deep-time ocean–atmosphere evolution. Earth Planet. Sci. Lett. 389, 209–220.
Lehrmann, D.J., Stepchinski, L., Altiner, D., Orchard, M.J., Montgomery, P., Enos, P., Ellwood, B.B., Bowring, S.A., Ramezani, J., Wang, H., Wei, J., Yu, M., Griffiths, J.D., Minzoni, M., Schaal, E.K., Li, X., Meyer, K.M., Payne, J.L., 2015. An integrated biostratigraphy (conodonts and foraminifers) and chronostratigraphy (paleomagnetic reversals, magnetic susceptibility, elemental chemistry, carbon isotopes and geochronology) for the Permian-Upper Triassic strata of Guandao section, Nanpanjiang Basin, south China. J. Asian Earth Sci. 108, 117–135.
Li, R., Chen, H., Xia, X., Yang, Q., Li, L., Xu, J., Huang, C., Danyushevsky, L.V., 2017. Ore fluid evolution in the giant Marcona Fe-(Cu) deposit, Perú: Evidence from in-situ sulfur isotope and trace element geochemistry of sulfides. Ore Geol. Rev. 86, 624–638.
Li, R., Chen, H., Xia, X., Yang, Q., Danyushevsky, L.V., Lai, C., 2018. Using integrated in-situ sulfide trace element geochemistry and sulfur isotopes to trace ore-forming fluids: Example from the Mina Justa IOCG deposit (southern Perú). Ore Geol. Rev. 101, 165–179.
Li, R., Chen, H., Large, R.R., Zhao, L., Liu, Y., Jiao, J., Xia, X.-P., Yang, Q., 2020b. Ore-forming fluid source of the orogenic gold deposit: Implications from a combined pyrite texture and geochemistry study. Chem. Geol. 552, 119781.
Li, J.-X., Hu, R.-Z., Zhao, C.-H., Zhu, J.-J., Huang, Y., Gao, W., Li, J.-W., Zhuo, Y.-Z., 2020a. Sulfur isotope and trace element compositions of pyrite determined by

NanoSIMS and LA-ICP-MS: new constraints on the genesis of the Shuiyindong Carlin-like gold deposit in SW China. Miner. Deposita 55 (7), 1279–1298.
Li, J., Zhao, C., Huang, Y., Zhuo, Y., Li, J., 2019. In-situ sulfur isotope and trace element of pyrite constraints on the formation and evolution of the Nibao Carlin-type gold deposit in SW China. Acta Geochimica. 38 (4), 555–575.
Liang, P., Chen, L.i., Li, R., Xie, Y., Wu, C., Lai, C.-K., 2021. In-situ element geochemical and sulfur isotope signature of pyrite and chalcopyrite: Constraints on ore-forming processes of the Laoshankou iron oxide-copper (-gold) deposit, northern East Junggar. Ore Geol. Rev. 139, 104510.
Liang, J., Li, J., Liu, X., Zhai, W., Huang, Y.i., Zhao, J., Sun, W., Song, M., Li, J., 2020. Multiple element mapping and in-situ S isotopes of Au-carrying pyrite of Shuiyindong gold deposit, southwestern China using NanoSIMS: Constraints on Au sources, ore fluids, and mineralization processes. Ore Geol. Rev. 123, 103576.
Lin, S., Hu, K., Cao, J., Bai, T., Liu, Y., Han, S., 2021. An in situ sulfur isotopic investigation of the origin of Carlin-type gold deposits in Youjiang Basin, southwest China. Ore Geol. Rev. 134, 104187.
Lin, Z., Sun, X., Peckmann, J., Lu, Y., Xu, L.i., Strauss, H., Zhou, H., Gong, J., Lu, H., Teichert, B.M.A., 2016. How sulfate-driven anaerobic oxidation of methane affects the sulfur isotopic composition of pyrite: A SIMS study from the South China Sea. Chem. Geol. 440, 26–41.
Lin, Y., Wu, N., Li, D.a., Ling, H.-F., 2020. Heterogeneity in the Ediacaran-Cambrian coastal oceans: a sulphur isotope perspective. Geol. Mag. 157 (7), 1112–1120.
Liu, Y., 2019. The Genesis of the Nibao Gold Deposit in Pu'an Country. Chengdu University of Technology, Guizhou province.
Liu, S., Su, W., Hu, R., Feng, C., Gao, S., Coulson, I.M., Wang, T., Feng, G., Tao, Y., Xia, Y., 2010. Geochronological and geochemical constraints on the petrogenesis of alkaline ultramafic dykes from southwest Guizhou Province, SW China. Lithos. 114 (1-2), 253–264.
Liu, J., Tran, M.-D., Tang, Y., Nguyen, Q.-L., Tran, T.-H., Wu, W., Chen, J., Zhang, Z., Zhao, Z., 2012. Permo-Triassic granitoids in the northern part of the Truong Son belt, NW Vietnam: Geochronology, geochemistry and tectonic implications. Gondw. Res. 22 (2), 628–644.
Liu, H., Wang, Y., Fan, W., Zi, J., Cai, Y., Yang, G., 2014. Petrogenesis and tectonic implications of Late-Triassic high ε Nd (t)-ε Hf (t) granites in the Ailaoshan tectonic zone (SW China). Sci. China Earth Sci. 57 (9), 2181–2194.
Maohong, C., Jingwen, M., Bierlein, F.P., Norman, T., Uttley, P.J., 2011a. Structural features and metallogenesis of the Carlin-type Jinfeng (Lannigou) gold deposit, Guizhou Province, China. Ore Geol. Rev. 43 (1), 217–234.
McLennan, S.M., 2001. Relationships between the trace element composition of sedimentary rocks and upper continental crust. Geochem. Geophys. Geosyst. 2 (4).
Molnár, F., Mänttäri, I., O'Brien, H., Lahaye, Y., Pakkanen, L., Johanson, B.o., Käpyaho, A., Sorjonen-Ward, P., Whitehouse, M., Sakellaris, G., 2016. Boron, sulphur and copper isotope systematics in the orogenic gold deposits of the Archaean Hattu schist belt, eastern Finland. Ore Geol. Rev. 77, 133–162.
Ohmoto, H., Goldhaber, M.B., 1997. Sulfur and carbon isotopes. In: Barnes, H.L. (Ed.), Geochemistry of Hydrothermal Ore Deposits, third ed. J Wiley and Sons, New York, pp. 517–611.
Pi, Q., Hu, R., Xiong, B., Li, Q., Zhong, R., 2017. In situ SIMS U-Pb dating of hydrothermal rutile: reliable age for the Zhesang Carlin-type gold deposit in the golden triangle region, SW China. Mineral. Deposita. 52 (8), 1179–1190.
Sakai, H., 1968. Isotopic properties of sulfur compounds in hydrothermal processes. Geochem. J. 2 (1), 29–49.
Seal, R.R., 2006. Sulfur isotope geochemistry of sulfide minerals. Sulfide Mineralolgy and Geochemistry. 61 (1), 633–677.
Shen, Y., Farquhar, J., Zhang, H., Masterson, A., Zhang, T., Wing, B.A., 2011. Multiple S-isotopic evidence for episodic shoaling of anoxic water during Late Permian mass extinction. Nat. Commun. 2, 210.
Shu, L., Yao, J., Wang, B.o., Faure, M., Charvet, J., Chen, Y., 2021. Neoproterozoic plate tectonic process and Phanerozoic geodynamic evolution of the South China Block. Earth Sci. Rev. 216, 103596.
Su, W., Heinrich, C.A., Pettke, T., Zhang, X., Hu, R., Xia, B., 2009. Sediment-hosted gold deposits in Guizhou, China: Products of Wall-Rock Sulfidation by Deep Crustal Fluids. Econ. Geol. 104 (1), 73–93.
Su, W., Dong, W., Zhang, X.-C., Shen, N., Hu, R.-z., Hofstra, A.H., et al., 2018. Carlin-type gold deposits in the Dian-Qian-Gui "Golden Triangle" of southwest China. Rev. Econ. Geol. 157–185.
Sykora, S., Cooke, D.R., Meffre, S., Stephanov, A.S., Gardner, K., Scott, R., et al., 2018. Evolution of pyrite trace element compositions from porphyry-style and epithermal conditions at the lihir gold deposit: implications for ore genesis and mineral processing. Econ. Geol. 113, 193–208.
Tan, Q.-P., Xia, Y., Xie, Z.-J., Yan, J., 2015a. Migration paths and precipitation mechanisms of ore-forming fluids at the Shuiyindong Carlin-type gold deposit, Guizhou. China. Ore Geology Reviews. 69, 140–156.
Tan, Q.-P., Xia, Y., Xie, Z.-J., Yan, J., Wei, D., 2015b. S, C, O, H, and Pb isotopic studies for the Shuiyindong Carlin-type gold deposit, Southwest Guizhou, China: constraints for ore genesis. Chin. J. Geochem. 34 (4), 525–539.
Ulrich, T., Long, D.G.F., Kamber, B.S., Whitehouse, M.J., 2011. In Situ Trace Element and Sulfur Isotope Analysis of Pyrite in a Paleoproterozoic Gold Placer Deposit, Pardo and Clement Townships, Ontario. Canada. Economic Geology. 106 (4), 667–686.
Wang, Y., Wang, L., Zhang, M., Wang, L., 1995. Texture of the Upper Crust and Pattern of the Disseminated Gold Deposits Distributed in Nanpanjiang Area. Guizhou Geology. 12, 91–183.
Wang, Y., Han, X., Petersen, S., Frische, M., Qiu, Z., Li, H., Li, H., Wu, Z., Cui, R., 2017. Mineralogy and trace element geochemistry of sulfide minerals from the Wocan Hydrothermal Field on the slow-spreading Carlsberg Ridge, Indian Ocean. Ore Geol. Rev. 84, 1–19.
Wang, Z., Xu, D., Zhang, Z., Zou, F., Wang, L.i., Yu, L., Hu, M., 2015. Mineralogy and trace element geochemistry of the Co- and Cu-bearing sulfides from the Shilu Fe–Co–Cu ore district in Hainan Province of South China. J. Asian Earth Sci. 113, 980–997.
Wei, D.-T., Xia, Y., Gregory, D.D., Steadman, J.A., Tan, Q.-P., Xie, Z.-J., Liu, X.-J., 2020. Multistage pyrites in the Nibao disseminated gold deposit, southwestern Guizhou Province, China: Insights into the origin of Au from textures, in situ trace elements, and sulfur isotope analyses. Ore Geol. Rev. 122, 103446.
Wei, D.-T., Zhou, T.-F., Xia, Y., Fan, Y.u., Xie, Z.-J., Liu, X.-J., Tan, Q.-P., Bai, L.-A., Wang, F.-Y., 2022. Pyrite textural, trace elemental and sulfur isotope signatures of the Badu gold deposit, Youjiang basin (SW China): Implications for ore-fluid source and Au precipitation mechanism. Ore Geol. Rev. 149, 105083.
Westrich, J.T., Berner, R.A., 1984. The role of sedimentary organic matter in bacterial sulfate reduction: The G model tested1. Limnol. Oceanogr. 29 (2), 236–249.
Wu, Y.-F., Evans, K., Fisher, L.A., Zhou, M.-F., Hu, S.-Y., Fougerouse, D., Large, R.R., Li, J.-W., 2020. Distribution of trace elements between carbonaceous matter and sulfides in a sediment-hosted orogenic gold system. Geochim. Cosmochim. Acta 276, 345–362.
Wu, N., Farquhar, J., Strauss, H., Kim, S.-T., Canfield, D.E., 2010. Evaluating the S-isotope fractionation associated with Phanerozoic pyrite burial. Geochim. Cosmochim. Acta 74 (7), 2053–2071.
Xie, Z., Xia, Y., Cline, J., Koenig, A., Wei, D., Tan, Q., et al., 2018a. Are there carlin-type gold deposits in China? A comparison of the Guizhou, China, Deposits with Nevada, USA, deposits. Rev. Econ. Geol. 187–233.
Xie, Z., Xia, Y., Cline, J.S., Pribil, M.J., Koenig, A., Tan, Q., et al., 2018b. Magmatic origin for sediment-hosted Au deposits, Guizhou Province, China. In Situ chemistry and sulfur isotope composition of pyrites, Shuiyindong and Jinfeng deposits. Econ. Geol. 113, 1627–1652.
Xie, Z., Huang, K.-J., Xia, Y., Cline, J., Tan, Q., Liu, J., Xiao, J., Yan, B., 2022. Heavy δ26Mg values in carbonate indicate a magmatic-hydrothermal origin of Carlin-type Au deposit. Geochim. Cosmochim. Acta 333, 166–183.
Xu, L., Lehmann, B., Mao, J., 2013. Seawater contribution to polymetallic Ni–Mo–PGE–Au mineralization in Early Cambrian black shales of South China: Evidence from Mo isotope, PGE, trace element, and REE geochemistry. Ore Geol. Rev. 52, 66–84.
Yan, J., Hu, R., Liu, S., Lin, Y., Zhang, J., Fu, S., 2018. NanoSIMS element mapping and sulfur isotope analysis of Au-bearing pyrite from Lannigou Carlin-type Au deposit in SW China: New insights into the origin and evolution of Au-bearing fluids. Ore Geol. Rev. 92, 29–41.
Yang, L., Wang, Q., Large, R.R., Fougerouse, D., Mukherjee, I., Zhang, Q., Deng, J., 2022. Texture and geochemistry of pyrite from the Jinya, Nakuang and Gaolong gold deposits in the Youjiang Basin: implications for basin-scale gold mineralization. Miner. Deposita 57 (8), 1367–1390.
Zhang, Y.-M., Gu, X.-X., Bai, X., Liu, R.-P., Zheng, G., Tun, C.-B., et al., 2013. Sulfur and lead isotopic composition characteristics of the Zhesang gold deposit in Funing County. Yunnan. Earth Science Frontiers. 20, 32–39.
Zhang, P., Huang, X.-W., Cui, B., Wang, B.-C., Yin, Y.-F., Wang, J.-R., 2016. Re-Os isotopic and trace element compositions of pyrite and origin of the Cretaceous Jinchang porphyry Cu-Au deposit, Heilongjiang Province, NE China. J. Asian Earth Sci. 129, 67–80.
Zhang, J., Lin, Y., Yan, J., Li, J., Yang, W., 2017. Simultaneous determination of sulfur isotopes and trace elements in pyrite with a NanoSIMS 50L. Anal. Methods 9 (47), 6653–6661.
Zhao, J., Liang, J., Li, J., Huang, Y.i., Liu, X., Zhang, J., Hao, J., Sun, W., Li, J., Xie, J., 2020. Gold and sulfur sources of the Taipingdong Carlin-type gold deposit: Constraints from simultaneous determination of sulfur isotopes and trace elements in pyrite using nanoscale secondary ion mass spectroscopy. Ore Geol. Rev. 117, 103299.
Zheng, L., Yang, R., Liu, J., Gao, J., Chen, J., Cheng, W., 2019. Geological-geochemical characteristics and genesis of the large Nibao gold deposit in southwestern Guizhou. Geological Review. 65, 1363–1382.
Zi, J.-W., Cawood, P.A., Fan, W.-M., Wang, Y.-J., Tohver, E., McCuaig, T.C., Peng, T.-P., 2012. Triassic collision in the Paleo-Tethys Ocean constrained by volcanic activity in SW China. Lithos 144-145, 145–160.